

GA-A23255

**MHD INSTABILITIES OCCURRING NEAR/AT  
THE TRANSPORT BARRIER, INCLUDING  
LOSS OF CONFINEMENT IN H-MODES**

by  
L.L. LAO

**SEPTEMBER 1999**

## DISCLAIMER

This report was prepared as an account of work sponsored by an agency of the United States Government. Neither the United States Government nor any agency thereof, nor any of their employees, makes any warranty, express or implied, or assumes any legal liability or responsibility for the accuracy, completeness, or usefulness of any information, apparatus, product, or process disclosed, or represents that its use would not infringe privately owned rights. Reference herein to any specific commercial product, process, or service by trade name, trademark, manufacturer, or otherwise, does not necessarily constitute or imply its endorsement, recommendation, or favoring by the United States Government or any agency thereof. The views and opinions of authors expressed herein do not necessarily state or reflect those of the United States Government or any agency thereof.

**MHD INSTABILITIES OCCURRING NEAR/AT  
THE TRANSPORT BARRIER, INCLUDING  
LOSS OF CONFINEMENT IN H-MODES**

by  
**L.L. LAO**

This is a preprint of a paper presented at the Seventh International Atomic Energy Agency Technical Committee Meeting on H-Mode and Transport Barrier Physics, September 27-29, 1999 in Oxford, United Kingdom and to be published in *Plasma Physics and Controlled Fusion*.

Work supported by  
the U.S. Department of Energy  
under Contract No. DE-AC03-99ER54463

**GA PROJECT 30033  
SEPTEMBER 1999**

## **ABSTRACT**

In configurations with transport barriers the improved edge and core confinement leads to large pressure gradient and large edge bootstrap current density which often drive magnetohydrodynamic (MHD) instabilities terminating the discharge or reducing the discharge performance. The edge and the core transport barriers deteriorate or are completely lost. In this presentation, recent experimental and theoretical developments concerning MHD instabilities occurring near/at the edge and the core transport barriers are summarized emphasizing the dominant instabilities and the comparison with theory.

## I. INTRODUCTION

One of the major objectives of advanced tokamak research is to develop plasma configurations with high confinement and improved stability at high  $\beta$ . Two of the more promising enhanced confinement regimes are the H- and VH-mode configurations [1,2] which exhibit improved confinement in the plasma edge, and the negative-central/optimized shear (NCS/OS) configuration [3,4] which shows improved confinement in the plasma core. The improved edge and core confinement leads to large pressure gradient  $P'$  and large edge bootstrap current density  $J_{BS}$  which often drive magnetohydrodynamic (MHD) instabilities terminating the discharge or reducing the discharge performance. The edge and the core transport barriers deteriorate or are completely lost. In this presentation, recent experimental and theoretical developments concerning MHD instabilities occurring near/at the edge and the core transport barriers are summarized, emphasizing the dominant instabilities observed in H-mode, VH-mode, and NCS/OS discharges and the comparison with theory.

In the area of edge instabilities, new developments since the last two comprehensive reviews [5,6] include characterization and modification of edge instabilities using methods such as plasma shaping, impurity injection, and current ramp down [7-9]. The goals here are to develop a means to control the edge  $P'$  and  $J_{BS}$  as well as to improve the understandings of these instabilities. Despite its simplicity and various assumptions, predictions based on high toroidal mode number,  $n$ , ideal ballooning theory are consistent with observed changes in pressure gradients and edge localized mode (ELM) character when second regime access is included. However, edge instabilities/ELMs cannot be explained by a simple instability to high  $n$  ideal ballooning modes. A working hypothesis for edge-instabilities/ELMs is that they are ballooning/kink/peeling modes arising from an interaction among MHD modes with various  $n$  and the evolution and growth of the edge  $P'$  and  $J_{BS}$ . Predictions from this working model are consistent with experimental results. Detailed low  $n = 1-5$  ideal stability analyses using simulated and accurately reconstructed experimental equilibria suggest that discharges with large edge  $P'$  and  $J_{BS}$  are more unstable to  $n > 1$  modes with a large peeling component [10-12]. Consistent with the experimental observations from several tokamaks, [13-15], simulation results suggest that the stability improves with triangularity [12]. Other developments include studies of the diamagnetic stabilization effects on the high  $n$  ideal ballooning modes [16], and coupled high  $n$  peeling-ballooning modes [17]. Results based on 3-D simulations of Braginskii equations and simple analytic models indicate that diamagnetic effects are strongly stabilizing when the edge pressure pedestal width is narrow [16]. This may contribute to the large edge pressure gradients often observed in H- and VH-mode discharges.

In the area of core instabilities, the devastating  $n = 1$  instabilities often terminating NCS/OS discharges with peaked pressure profiles are explained well by ideal stability theory and can be avoided by reducing the pressure peakedness as theoretically suggested. The ideal-like growth times observed in DIII-D [18] can be explained by driven ideal instabilities with the growth time modified by the plasma heating time as the instabilities are driven slowly through their instability threshold [19]. Preceding these ideal termination events, localized and global resistive modes such as resistive interchange and tearing modes are also sometime observed and may contribute to the termination [18,20]. These resistive modes are less well understood than the ideal instabilities. Other core transport barrier related ideal instabilities include the low  $n$  barrier localized modes (BLM) observed in JT-60U high- $\beta_p$  mode discharges [21].

Other resistive instabilities which are not addressed here but are important for steady state high performance include resistive wall modes [22] and neoclassical tearing modes [23].

In Section II, recent developments concerning edge instabilities are summarized. Recent developments in core instabilities are discussed in Section III. A summary is given in Section IV.

## 2. MHD INSTABILITIES ASSOCIATED WITH EDGE TRANSPORT BARRIERS

Edge instabilities often appear as cycles of edge localized mode (ELM) [5,6] with varying amplitudes and frequency depending on the edge conditions, the power loss from the core, the safety factor  $q$ , and the plasma shape. The instabilities can have effects ranging from a slight decrease of the edge density and temperature leading to a saturation of the normalized beta  $\beta_N$ , to a drop of density and temperature across the entire plasma with a decrease in  $\beta_N$ . ELMs have been observed in H- and VH-mode discharges with various poloidal cross sections including single- and double-null divertor, Dee and crescent shapes [11] and various current profiles over a wide range of  $\beta_N = 2.0\text{--}5.0$  [24]. With the appearance of the large amplitude Type I ELM, the edge and the core transport barriers often deteriorate or are lost. The attainable beta values decrease with the fraction of plasma current contained in the plasma edge region [24] and are consistent with the previously observed DIII-D operational beta limit of  $\beta_N \leq 4 I_i$  [25,26]. Here,  $I_i$  is the plasma internal inductance which measures the peakedness of the current density  $J$  profile and decreases as edge  $J$  increases.

The performance of H- and VH-mode discharges is often limited and degraded by these edge instabilities. This is illustrated in Fig. 1, where the time evolution of a DIII-D double-null divertor H-mode discharge is shown [11]. As shown in the figure, the giant Type I ELM causes a rapid drop of the edge electron temperature  $T_e$  and a decrease of the global  $\beta_N$ . As subsequent ELMs occur, the edge  $T_e$  and  $\beta_N$  continue to decrease. Prior to the first giant Type I ELM, magnetic oscillations with  $n = 2\text{--}9$  are sometime observed [10–11,18,27]. The oscillations are highly localized spatially with a very short time duration. This is illustrated in Fig. 2 for the DIII-D discharge shown in Fig. 1 [18]. The oscillations have a wavelength which corresponds to  $n \approx 5$  and a fast ideal-like growth time of  $\gamma^{-1} \approx 150 \mu\text{s}$ . They rotate in the electron diamagnetic direction which is consistent with localization in the plasma edge region. They have a strong ballooning character localized poloidally in the bad curvature region. After this first giant ELM, the discharge usually evolves into a quasi-stationary phase at similar or lower  $\beta_N$  values. Magnetic precursors are usually not observed during this phase in DIII-D, but magnetic precursors with  $n = 3\text{--}6$  have been observed under similar conditions in ASDEX-U [27].

In addition to ELM, other edge instabilities include outer modes (OM), which are low  $n$  current-driven kink/peeling modes [28]. These are mostly observed in JET and can also strongly degrade the plasma performance [9,28]. The modes are observed around and outside the safety factor  $q = 3$  surface and usually have  $n = 1$ . Outer modes cause a small and slow increase in the  $D_\alpha$  radiation signal which is quite distinct from that of an ELM. This is

illustrated in Fig. 3 for a JET hot-ion H-mode discharge [9]. As shown in the figure, the rate of rise of the plasma stored energy and the neutron rate are limited by a  $n = 1$  outer mode starting at 12.9 s. A similar  $n = 1$  fast edge mode has also been observed in some C-Mod EDA discharges [29].

In several tokamaks the edge  $P'$  and the pedestal energy are observed to increase with the triangularity of the plasma shape  $\delta$  [13–15]. This is illustrated in Fig. 4 for a set of JT-60U data prior to the onset of ELMs [13] and an ASDEX-U discharge during the ELMing phase [14]. Here, the normalized pressure gradient  $\alpha = \mu_0 P'(\psi)(V/4\pi R_0)^{1/2}$  and the normalized core and pedestal plasma energy at various  $\delta$  are compared. Similar increase of edge  $P'$  with triangularity is also observed in DIII-D [15]. This is illustrated in Fig. 5, where the normalized edge electron pressure gradients  $\alpha_e$  for a set moderate density DIII-D ELMing single-null divertor discharges at various upper triangularity  $\delta_{\text{UPPER}}$  are compared. As shown in the figure,  $\alpha_e$  increases strongly with  $\delta_{\text{UPPER}}$ .

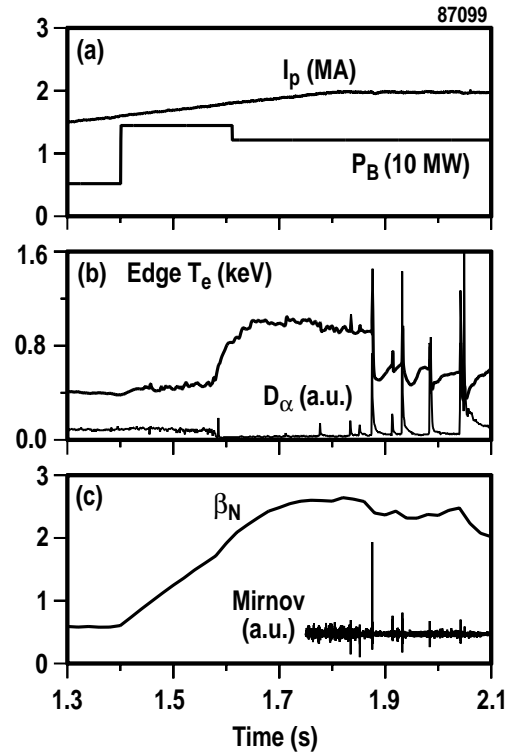


FIG. 1. Time evolution of a DIII-D H-mode discharge: (a) plasma current and neutral beam injection power, (b) edge electron temperature near  $\rho = 0.9$  and divertor  $D_\alpha$  radiation; (c) normalized toroidal beta and Mirnov oscillations in the outboard midplane region.

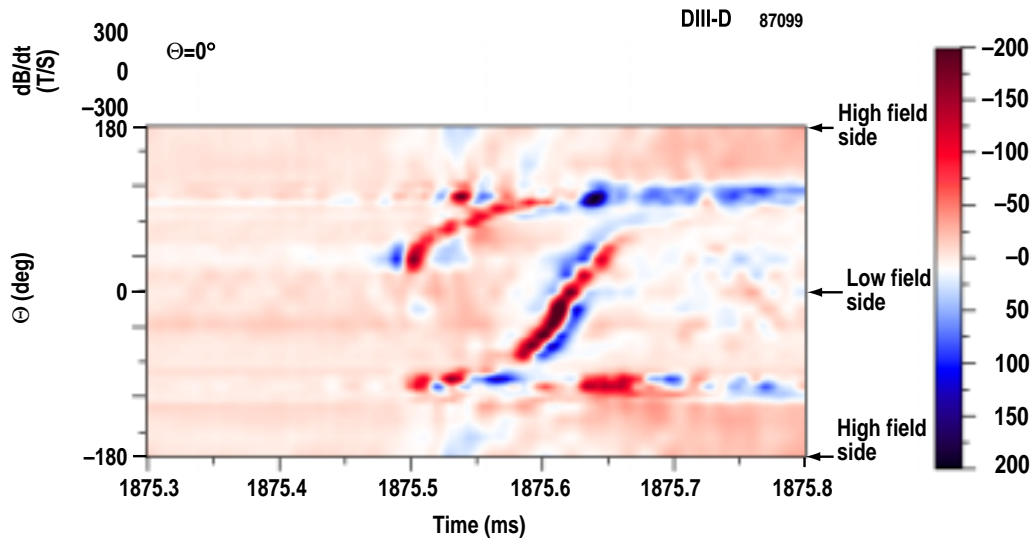


FIG. 2. Time evolution of  $dB_\theta/dt$  from a magnetic probe at the outboard (low field side) midplane and contour plot of  $dB_\theta/dt$  versus time and poloidal angle for a DIII-D H-mode discharge.

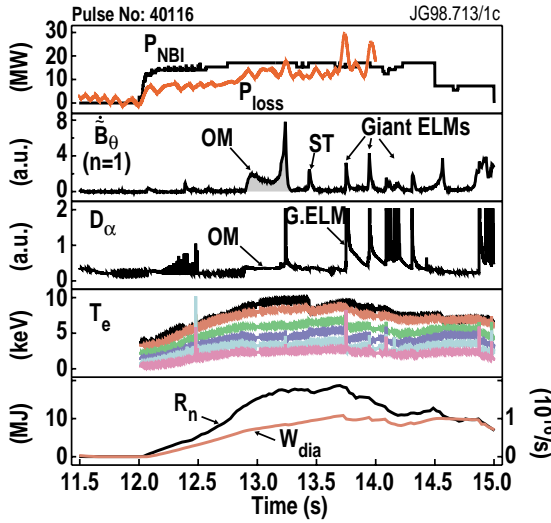


FIG. 3. Temporal evolution of a deuterium JET ELM-free hot-ion H-mode discharge where the rates of rise of the plasma stored energy and the neutron rate are limited by an outer mode (OM) and a giant ELM.

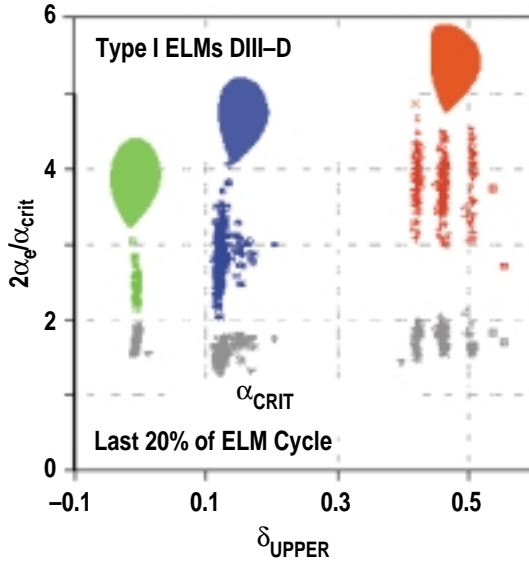


FIG. 5. Normalized edge pressure gradient  $\alpha$  averaged over last 20% of ELM cycle as a function of the upper triangularity  $\delta_{\text{UPPER}}$  of the plasma shape for a set of moderate density DIII-D discharges. Also shown are the critical normalized pressure gradients  $\alpha_{\text{CRIT}}$  at the first ballooning stability limit near the nose of the stability boundary.

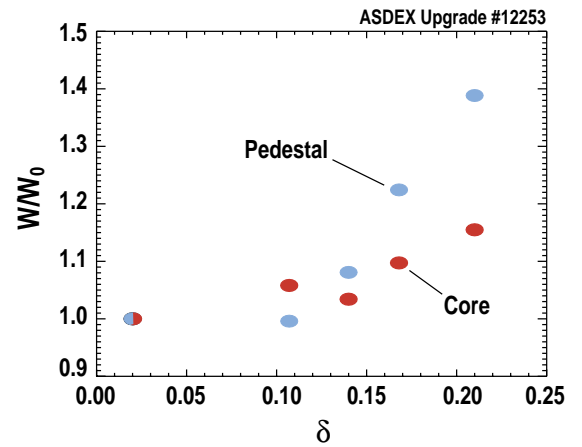
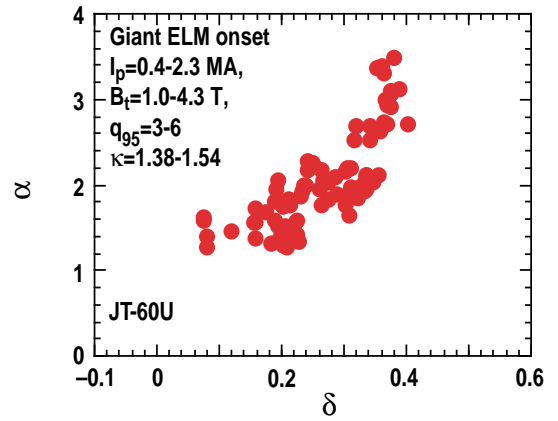


FIG. 4. Normalized edge pressure gradient  $\alpha$  at the onset of giant ELM as a function of the triangularity  $\delta$  of the plasma shape for a set of JT-60U discharges and normalized plasma pedestal and core stored energy as a function of  $\delta$  for an ELMing ASDEX-U discharge.

### A. High $n$ ideal ballooning modes

One of the central issues of edge instabilities is to improve the understanding of the physical mechanism and to identify the MHD instabilities which limit the edge  $P'$  and drive the instabilities. The first detailed edge  $P'$  measurements and comparison against predictions from high  $n$  ideal ballooning theory were made in DIII-D in

1988 [30]. The measurements were done using a high edge spatial resolution Thomson scattering system in single-null divertor deuterium plasmas with hydrogen beam. The edge  $P'$  are found to be near or above the first ideal ballooning stability limit before a giant Type I ELM and to fall below the limit after an ELM [30,31]. Other tokamaks have since reported similar observations although in less detail [5,6].

More recent results from DIII-D with deuterium beam show a much stronger edge transport barrier and a larger edge  $P'$  that substantially exceeds the first ballooning stability limit before Type I ELMs [11,32]. Stability analyses show that in these case the discharges have access to the second ballooning stability regime in the plasma outer edge region when the contribution of the edge  $J_{BS}$  is included in the equilibrium. Without edge  $J_{BS}$  the discharges have no access to the second ballooning stability regime and the edge  $P'$  substantially exceeds the first ballooning limit. This is illustrated in Fig. 5, where the ratio  $\alpha_e$  to the critical normalized first ballooning stability limit  $\alpha_e/\alpha_{CRIT}$  at various values of  $\delta$  are compared [15]. The variation of  $\alpha_{CRIT}$  with  $\delta$  is also shown in Fig. 5. As shown in the figure, the ratio  $2\alpha_e/\alpha_{CRIT}$  substantially exceeds 1 and increases with  $\delta$ , whereas  $\alpha_{CRIT}$  varies only weakly with  $\delta$ . Similar results on ballooning stability have also been reported for C-Mod EDA discharges [33]. These results indicate that edge instabilities cannot be explained by a simple picture of instability to the high  $n$  ideal ballooning modes. Rather, in these discharges the absence of high  $n$  ideal ballooning instabilities facilitating the growth of edge  $P'$  and  $J_{BS}$ , which destabilize other MHD modes.

These results also suggest that edge instabilities may be controlled by limiting the edge  $P'$  and  $J_{BS}$  through elimination of the second ballooning stability access in the edge region. Theoretical calculations indicate that second ballooning stability access in the plasma outer edge region is reduced at low and high squareness [34]. At low and high squareness, the amount of edge  $J_{BS}$  required to gain second ballooning stability access in the plasma edge is substantially larger than at moderate squareness.

Consistent with the results from these calculations, experimental results from DIII-D show that ELM amplitude and frequency can be varied by controlling access to the second ballooning stability regime at the edge through variation of the squareness of the discharge shape [35]. This is illustrated in Fig. 6, where the ELM frequency and amplitude as indicated by the divertor  $D_\alpha$  radiation and the change in edge  $T_e$  for a moderate and a high squareness DIII-D discharge are compared. As shown in the figure, at high squareness the ELM frequency is strongly increased and the amplitudes strongly reduced. The ELM behavior at low squareness (not shown) is similar. The normalized edge pressure gradients  $\alpha$  is also compared to the ballooning stability boundary in Fig. 6 at the two time slices indicated by the arrows. As expected, at moderate squareness the discharge has second stability access in the plasma outer edge and the edge  $P'$  substantially exceeds the first regime limit in the neighboring flux surfaces. At high squareness, the discharge has no second regime access, and the edge  $P'$  is bound by the first ballooning limit.

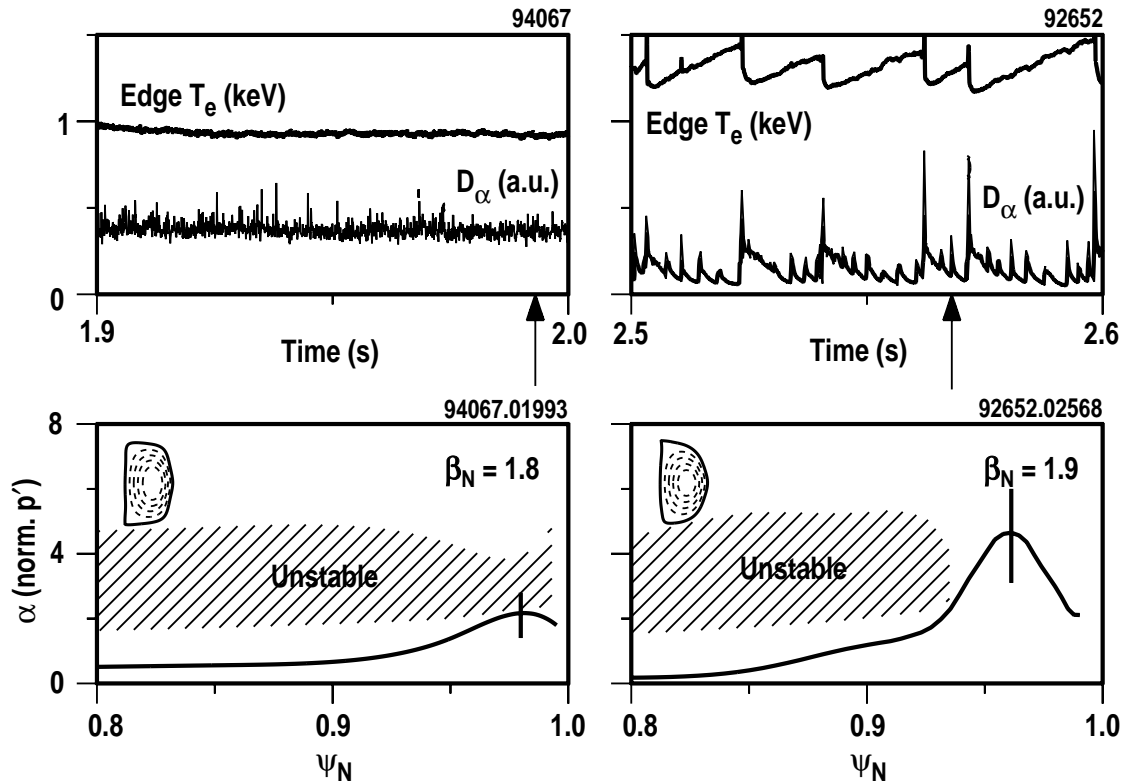


FIG. 6. Comparison of high  $n$  ideal ballooning stability, divertor  $D_\alpha$  signals, and edge electron temperatures for a high squareness and a moderate squareness DIII-D discharge. Arrows show time of stability calculations.

Recent results based on 3-D simulations of the Braginskii equations and simple analytic models suggest that diamagnetic effects may contribute to the stabilization of the high  $n$  ballooning modes when the edge pressure pedestal width  $\Delta$  is small [16]. This is illustrated in Fig. 7, where the critical edge  $P'$  against the high  $n$  ballooning modes are shown as a function of the normalized ion diamagnetic velocity  $V_{*i}$ . For small  $\Delta$ ,  $V_{*i}$  becomes much greater than 1 and the stability limit is much improved over that given by simple ideal ballooning theory. Also shown in Fig. 7 are three DIII-D single-null divertor H-mode data sets with increasing  $\delta$  [15]. As shown in the figure, the data show a general trend of increasing

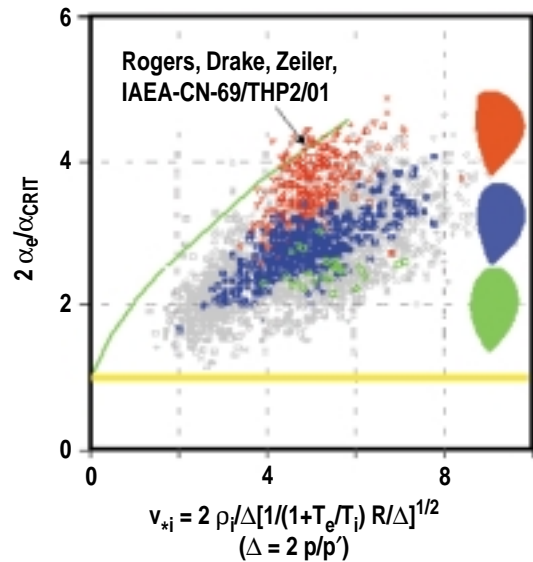


FIG. 7. Comparison of stability boundary for high  $n$  ideal ballooning modes when diamagnetic effects are included against three groups of DIII-D single-null divertor H-mode data sets with upper triangularity  $\delta_{\text{UPPER}} = -0.02, 0.13, \text{ and } 0.47$ .

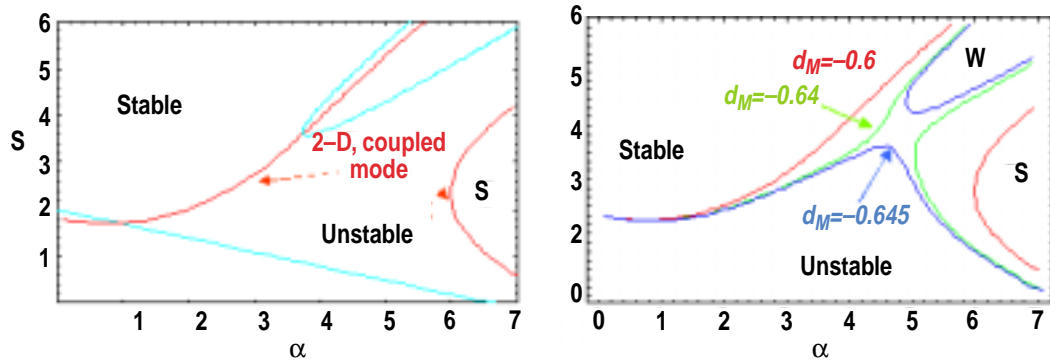


FIG. 8. A sequence of marginal stability curves from the 2-D stability calculation as the magnetic well is deepened from  $d_M = -0.6$  to  $d_M = -0.645$  showing access to second stability at the deepest well.

with  $V_{*i}$  which is in qualitative agreement with the simulation results. However, the theory cannot explain the increase of edge  $P'$  with  $\delta$ . Since the theory is presently restricted to circular geometry, further improvement of the theory to include the effects of plasma shape is needed in order to further test the theory.

The effects of peeling modes on second ballooning stability access have recently been studied [17]. With a shallow magnetic well, coupling between the peeling and the ballooning modes can prohibit second stability access. When the well is sufficiently deepened, second stability access becomes possible. This is illustrated in Fig. 8, where the marginal stability contours in the  $(S, \alpha)$  phase space from a 2-D stability calculations with different values of the magnetic well are compared. Here,  $D_M$  is a parameter describing the depth of the well and  $S$  is the magnetic shear. As shown in the figure, at  $D_M = -0.645$  the magnetic well is sufficiently deepened and second stability access becomes possible.

### B. Low $n$ ideal modes

As discussed in the previous section, edge instabilities cannot be explained by a simple picture of instability to high  $n$  ideal ballooning modes alone. In this section, recent studies concerning low  $n$  ideal kink/ballooning/peeling modes are summarized. These low  $n$  modes are driven unstable by both large edge  $P'$  and large edge  $J$ . This is illustrated in Fig. 9, where the growth rates  $\gamma$  against the ideal  $n = 1-3$  modes evaluated using the GATO code [36] for a set of simulated DIII-D VH-mode equilibria with various values of edge  $P'$  and

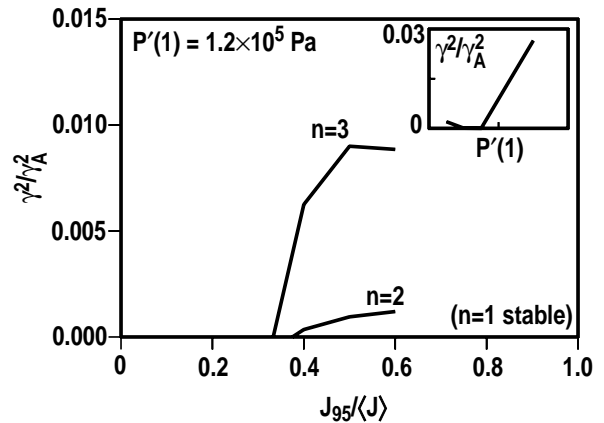


FIG. 9. Comparison of the growth rates of the ideal  $n = 1-3$  modes for a set of simulated DIII-D VH-mode equilibria with various values of edge current density. The variation of the growth rates with edge pressure gradient against the  $n = 3$  mode is given in the inset.

$J$  are compared [10]. As shown in the figure, as the normalized edge  $J$  at the 95% poloidal flux surface is increased, the  $n = 3$  modes become unstable first. With a further increase in edge  $J$ , the  $n = 2$  modes then become unstable. The  $n = 1$  modes are stable for all cases. Increasing edge  $P'$  has similar effects on the  $n = 1-3$  modes. The variation of  $\gamma$  against the  $n = 3$  modes as edge  $P'$  is increased is given in the inset. The radial structure of the unstable modes has a large edge-localized peeling component with a radial extent that increases with the edge pressure pedestal width. This is illustrated in Fig. 10. for a DIII-D NCS/OS H-mode discharge and a standard H-mode discharge [37]. As expected, the effects of ELMs are stronger on the NCS/OS H-mode discharge than the standard H-mode one.

The stability against these low  $n$  ideal modes improves with plasma triangularity  $\delta$  [12]. This is illustrated in Fig. 11, where the normalized growth rates against the  $n = 2-4$  modes

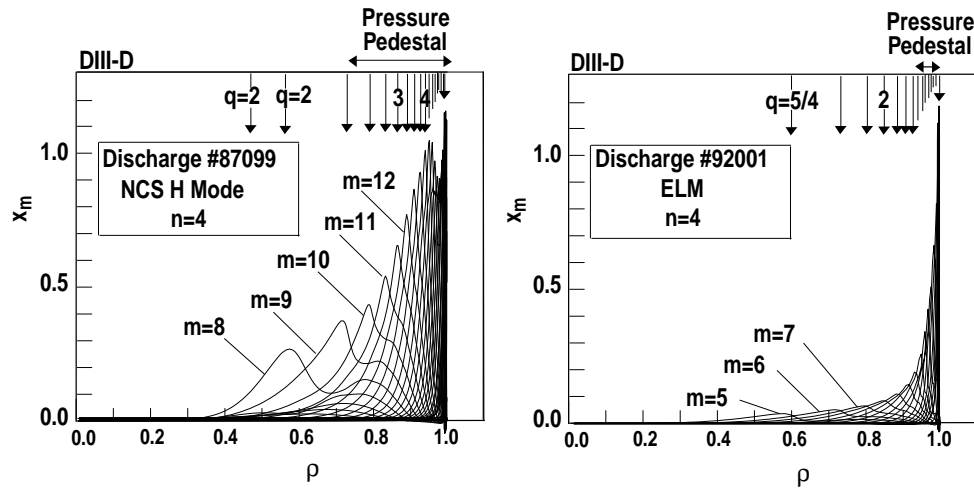


FIG. 10. Comparison of the radial structure of poloidal Fourier components of the unstable ideal  $n = 4$  modes for two DIII-D H-mode discharges with two different edge pressure pedestal widths.

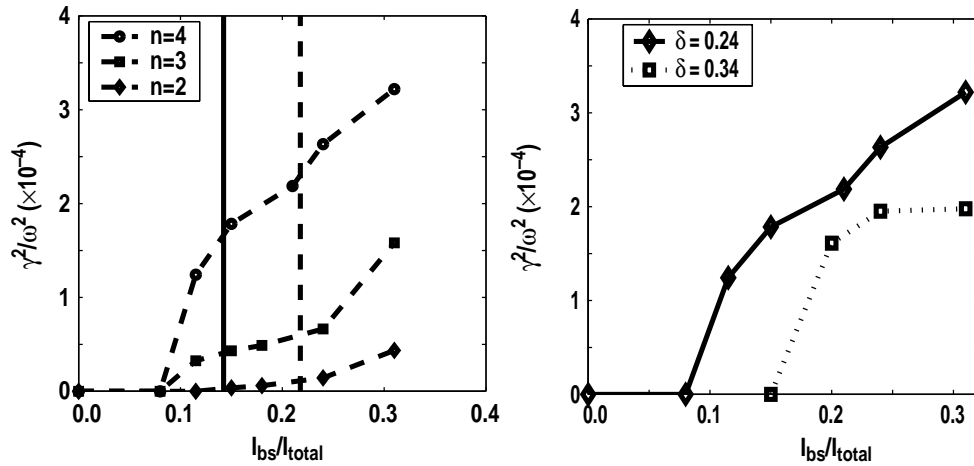


FIG. 11. Comparison of the growth rates against the ideal  $n = 2-4$  modes for a set of simulated ASDEX-U equilibria with various bootstrap current fraction. Vertical lines indicated experimental range of bootstrap current in ASDEX-U. Also shown are the growth rates against the  $n = 4$  mode at two different values of triangularity  $\delta$ .

fraction. Also shown are the growth rates against the  $n = 4$  modes at two different values of triangularity  $\delta$ . The  $n = 1$  modes are stable for all cases. As shown in the figure, modes with higher  $n$  tend to be more unstable and increasing  $\delta$  improves stability against these modes.

Results from current ramp-down experiments in JET show that outer modes (OM) are driven by current whereas ELMs are driven by pressure [9,38]. This is illustrated in Fig. 12 for two similar JET hot-ion H-mode discharges with and without current ramp-down. As shown in the figure, with current ramp-down the onset time for the OM is delayed by 500 ms but the giant Type I ELM occurs 300 ms earlier. The trajectories of these two discharges in the  $(\alpha, J)$  phase space at the 97% of the enclosed poloidal flux are also compared to the computed stability boundary against the high  $n$  ideal ballooning mode and the  $n = 1$  kink/peeling mode in Fig. 12 [38]. As shown in the figure, the discharge with current ramp-down is more stable to the kink/peeling mode, whereas the discharge without is more stable to ELMs.

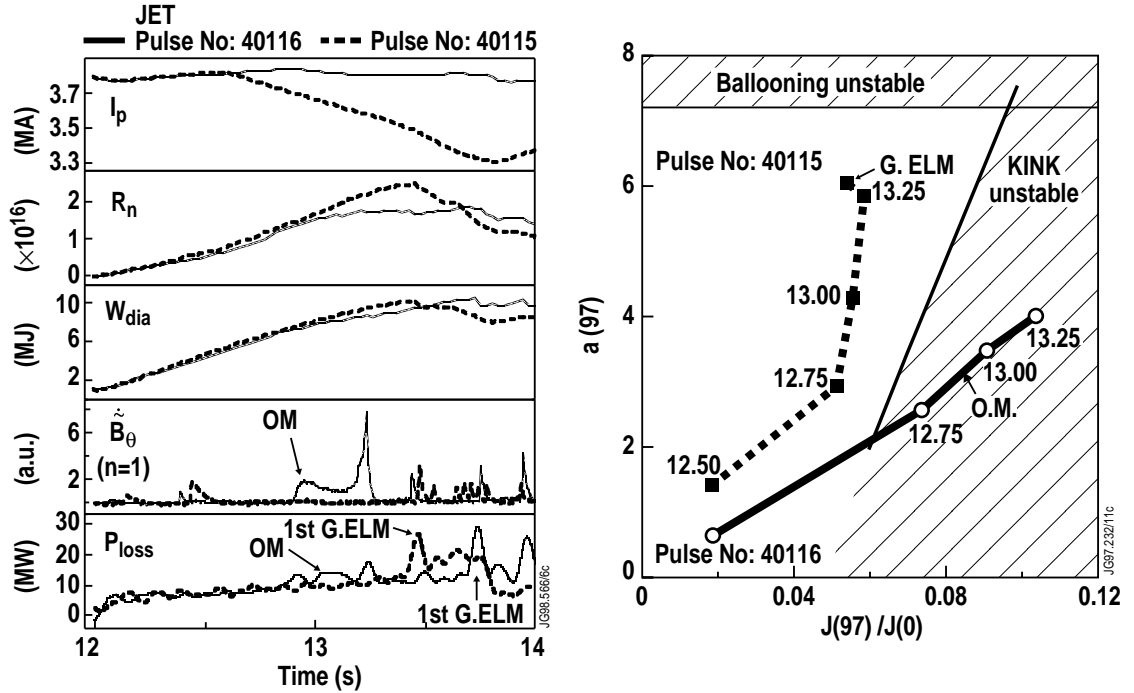


FIG. 12. Comparison of temporal evolution and trajectories in the normalized pressure-current  $(\alpha, J)$  phase space for two similar JET hot-ion H-mode discharges with and without current ramp-down. The trajectories of these two discharges in the  $(\alpha, J)$  phase space at the 97% of the enclosed poloidal flux are also compared to the computed stability boundary against the high  $n$  ballooning mode and the  $n = 1$  kink/peeling mode.

### C. Discussion

These recent theoretical and experimental results provide further support to the working hypothesis that edge-instabilities/ELMs are kink/ballooning/peeling modes arising from a complex interaction among MHD modes with various  $n$  and the evolution and growth of

edge  $P'$  and  $J$ . As the edge transport barrier is formed,  $P'$  is increased. This leads to an increase of  $J_{BS}$  which at some critical value will lead to an opening of the second ballooning stability zone. In turn this will allow a further increase of  $P'$ . The cycle will be repeated until an instability occurs at a lower  $n$ . Alternatively, the diamagnetic effects may provide the stabilization to the high  $n$  ballooning modes. Note that kink/peeling modes may become unstable before the second ballooning stability zone is open, as in the case of outer modes (OM). The supporting evidences for this model are: (1) the intermediate to low  $n > 1$  magnetic precursors sometime observed before ELM in DIII-D and ASDEX-U [10-11,18,27]; (2) Predictions based on this model are consistent with observed changes in edge  $P'$  and ELM character in DIII-D squareness experiments [34,35]; (3) Predictions based on this model are consistent with the improvement of edge  $P'$  with  $\delta$  and with current [9,12-15,38]. Some of the issues and needs are: (1) Magnetic precursors are not always observed, better detection and interpretation techniques are needed; (2) Computational tools to accurately compute  $n > 6$  modes and to study the nonlinear coupling between high and low  $n$  modes are not yet available; (3) More accurate edge  $J$  measurements and analysis are needed.

### 3. MHD INSTABILITIES ASSOCIATED WITH CORE TRANSPORT BARRIERS

The NCS/OS configuration is first observed in the TFTR and the DIII-D tokamak [3,4]. After the discovery, it is quickly recognized that the improved core confinement, although beneficial, can lead to very strong pressure profile peaking that terminates the discharge at relatively low  $\beta$  values. This is illustrated in Fig. 13 for a DIII-D and a JT-60U NCS/OS discharge with a L-mode edge. Here the temporal evolution of  $\beta_N$  and the D-D neutron production rate  $R_{DD}$  are shown [18,39]. The disruption is preceded by fast growing rotating magnetic precursors with  $n = 1$  and ideal-like growth times of  $\gamma^{-1} \sim 0.1\text{--}0.5$  ms for the DIII-D discharge and  $\gamma^{-1} \sim 0.01$  ms for the JT-60U discharge. The DIII-D growth time of  $\gamma^{-1} \sim 0.1\text{--}0.3$  ms is fast compared with the resistive growth time but slow compared with the ideal growth time. It is consistent with driven ideal MHD instabilities in which the growth times are modified by the plasma heating time as the instabilities are driven slowly through their instability threshold [19].

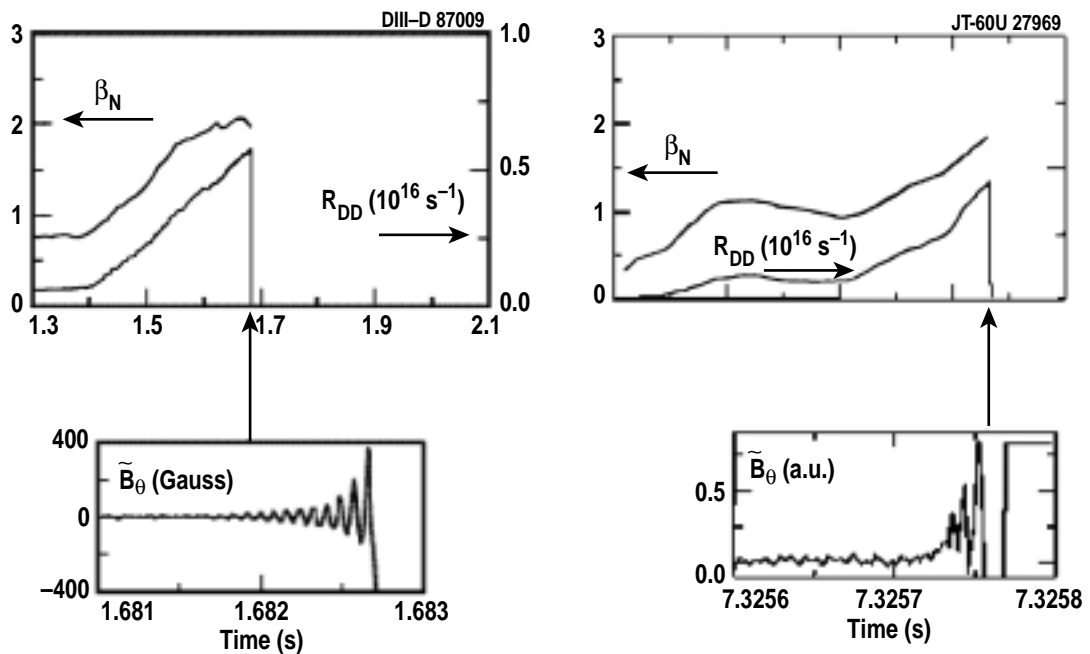


FIG. 13. Time traces of normalized beta  $\beta_N$  and neutron yield  $R_{DD}$  for a DIII-D and a JT-60U L-mode NCS/OS discharge showing a disruption preceded by a fast growing rotating  $n = 1$  magnetic precursor.

The  $n = 1$  instabilities terminating these discharges can be avoided by reducing the peakedness of the pressure profiles. The experimental  $\beta$  limit is consistent with the predicted dependence on the pressure profile peakedness based on ideal stability theory [40–43]. This is illustrated in Fig. 14 where the  $\beta_N$  values obtained at various  $P(0)/\langle P \rangle$  for a group of DIII–D and JET NCS/OS discharges are compared [40,42]. Also shown is the calculated ideal  $n = 1$  stability boundary [42,43]. The trajectories and the temporal evolution of several DIII–D and JET discharges are also given. In the DIII–D discharge, the pressure peakedness is reduced by L-H transition, whereas in the JET discharge it is reduced by delaying the main beam heating. Before these ideal termination events, localized and global resistive modes such as resistive interchange and tearing modes are also sometime observed and may contribute to the termination [18,20]. In JET discharges when these termination events are avoided,  $q = 2$  snakes and tearing modes may then appear [42].

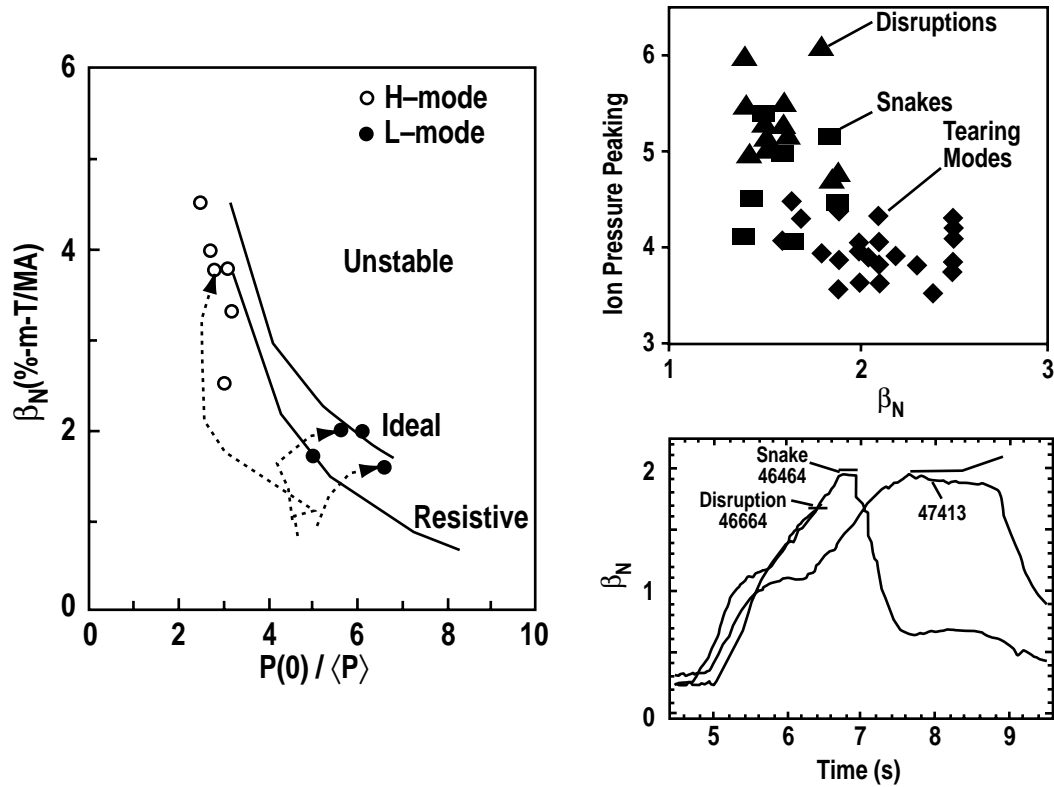


FIG. 14. Comparison of normalized beta  $\beta_N$  for a group of DIII–D and JET NCS/OS data set as a function of total and ion pressure profile peakedness. Also shown is the calculated ideal  $n = 1$  stability limit. For DIII–D the resistive  $n = 1$  limit is also shown. The trajectories and temporal evolution of several discharges are also given.

## 4. SUMMARY

Recent experimental and theoretical results are consistent with the working hypothesis that edge-instabilities/ELM are ballooning/kink/peeling modes arising from a complex interaction among MHD modes with various  $n$  and the evolution and growth of the edge  $P'$  and  $J_{BS}$ . Predictions based on high  $n$  ideal ballooning theory are consistent with observed changes in pressure gradients and ELM character when second ballooning regime access is included. When there is second stability access in the plasma edge, the edge  $P'$  is not bound by the first ballooning stability limit but is limited by some lower  $n$  mode. Diamagnetic effects may provide an alternative mechanism to stabilize the high  $n$  ballooning modes.

The  $n = 1$  instabilities often terminating the NCS/OS discharges with peaked pressure profiles are consistent with predictions based on ideal stability theory and can be avoided by reducing the pressure peakedness as theoretically suggested.

## REFERENCES

- [1] WAGNER F. *et al.* (1984) *Phys. Rev. Lett.* **53**, 1453.
- [2] JACKSON G. L. *et al.* (1991) *Phys. Rev. Lett.* **67**, 3098.
- [3] LEVINTON F. M. *et al.* (1995) *Phys. Rev. Lett.* **75**, 4417.
- [4] STRAIT E. J. *et al.* (1995) *Phys. Rev. Lett.* **75**, 4421.
- [5] ZOHN H. (1996) *Plasma Phys Control. Fusion* **38**, 105.
- [6] CONNOR J. W. (1998) *Plasma Phys. Control. Fusion* **40**, 531.
- [7] FERRON J. R. *et al.* (1999) *Proc. 26th EPS Conf. on Controlled Fusion and Plasma Physics*, Maastricht, The Netherlands (to be published), and General Atomics Report GA-A23156.
- [8] NAVE M. F. F. *et al.* (1999) *Proc. 26th EPS Conf. on Controlled Fusion and Plasma Physics*, Maastricht, The Netherlands (to be published).
- [9] NAVE M. F. F. *et al.* (1999) "Title needed here," JET Report JET-P(99)11, to be published in *Nucl. Fusion*.
- [10] STRAIT E. J. *et al.* (1993) *Proc. 20th EPS Conf. on Plasma Physics and Controlled Fusion Research*, Lisbon, Portugal, Vol. 17C, Part I, p. 211.
- [11] LAO L. L. *et al.* (1998) *Proc. 17th Int. Atomic Energy Fusion Energy Conf.*, Yokohama, Japan, to be published in *Nucl. Fusion*.
- [12] SAARELMA S. *et al.* (1999) *Proc. 26th EPS Conf. on Controlled Fusion and Plasma Physics*, Maastricht, The Netherlands (to be published); and (1999) H-mode Workshop.
- [13] KAMADA Y. *et al.* (1996) *Proc. 16th IAEA Conf. on Plasma Phys. and Contr. Nucl. Fusion Research*, Montreal, Canada, Vol. 1, p. 24.
- [14] WOLF R. C. *et al.* (1999), "Need a Title here," to be published in *Plasma Phys. Contr. Fusion*.
- [15] OSBORNE T. H. *et al.* (1999) H-Mode Workshop.
- [16] ROGER B. N. *et al.* (1999) *Phys. Plasmas* **6**, 2797.
- [17] WILSON H. R. and MILLER R. L. (1999) *Phys. Plasmas* **6**, 873.
- [18] STRAIT E. J. *et al.* (1997) *Phys. Plasmas* **4**, 1783.
- [19] CALLEN J. D. *et al.* (1999) *Phys. Plasmas* **6**, 2963
- [20] CHU M. S. *et al.* (1996) *Phys. Rev. Lett.* **77**, 2710.
- [21] TAKEJI S. *et al.* (1997) *Phys. Plasmas* **4**, 4283.
- [22] GAROFALO A. M. *et al.* (1999) *Phys. Rev. Lett.* **82**, 3811.
- [23] CHANG Z. *et al.* (1995) *Phys. Rev. Lett.* **74**, 4663.
- [24] LAO L. L. *et al.* (1997) *Proc. 24th EPS Conf. on Plasma Phys. and Contr. Fusion Research*, Berchtesgaden, Germany, Vol. 21A, Part III, p. 1117.

- [25] TAYLOR T. S. *et al.* (1990) *Proc. 13th IAEA Conf. on Plasma Phys. and Contr. Nucl. Fusion Research*, Washington, D.C., Vol. 1, p. 177.
- [26] STRAIT E. J. *et al.* (1991) *Proc. 18th EPS Conf. on Plasma Phys. and Contr. Fusion Research*, Berlin, Germany, Vol. 15C, Part II, p. 105.
- [27] MARASCHEK M. *et al.* (1998) *Proc. 25th EPS Conf. on Plasma Phys. and Contr. Fusion Research*, Berlin, Germany, Vol. 15C, Part II, p. 105.
- [28] NAVE M. F. F. *et al.* (1997) *Nucl. Fusion* **37**, 809.
- [29] HUTCHINSON I. H. *et al.* (1999) *Plasma Phys. Contr. Fusion* **41**, A609.
- [30] GOHIL P. **et al.** (1988) *Phys. Rev. Lett.* **61**, 1603.
- [31] LAO L. L. *et al.* (1989) *Plasma Phys. Contr. Fusion* **31**, 509.
- [32] OSBORNE T. H. *et al.* (1997) *Proc. 24th EPS Conf. on Plasma Phys. and Contr. Fusion Research*, Berchtesgaden, Germany, Vol. **21A**, Part III, p. 1101.
- [33] HUBBARD A. E. *et al.* (1998) *Phys. Plasmas* **5**, 1744
- [34] MILLER R. L. *et al.* (1998) *Plasma Phys. Contr. Fusion* **40**, 753.
- [35] FERRON J. R. *et al.* (1998), "Need a title here," submitted to *Nucl. Fusion*, and General Atomics Report GA-A22974.
- [36] BERNARD L. C. *et al.* (1981) *Comp. Phys. Commun.* **24**, 377.
- [37] TURNBULL A. D., private communication.
- [38] HUYSMANS G. T. A. *et al.* (1998) *Nucl. Fusion* **38**, 179.
- [39] ISHIDA S. *et al.* (1997) *Proc. 24th EPS Conf. on Plasma Phys. and Contr. Fusion Research*, Berchtesgaden, Germany, Vol. **21A**, Part II, 489.
- [40] LAO L. L. *et al.* (1996) *Phys. Plasmas* **3**, 1951.
- [41] ISHII Y. *et al.* (1998) *Plasma Phys. Contr. Fusion* **40**, 1607.
- [42] HENDER T. C. *et al.* (1999) *Proc. 26th EPS Conf. on Controlled Fusion and Plasma Physics*, Maastricht, The Netherlands (to be published).
- [43] TURNBULL A. D. *et al.* (1998) *Nucl. Fusion* **38**, 1467.

## **ACKNOWLEDGMENT**

This is a report of work supported by the U.S. Department of Energy under Contract No. DE-AC03-99ER54463.

I would like to thank the following people for their contribution to this paper: B. Alper, Yu.F. Baranov, P. Bonoli, V.S. Chan, M.S. Chu, J.R. Ferron, R.J. Groebner, S. Gunter, T.C. Hender, A.E. Hubbard, Y. Kamada, M.F.F. Nave, T.H. Osborne, M. Porkolab, B.N. Roger, S. Saarelma, E.J. Strait, S. Takeji, T.S. Taylor, A.D. Turnbull, H.R. Wilson, M.R. Wade, G.H. Wolf and S. Wolfe.